Efficient Li-Metal Plating/Stripping in Carbonate Electrolytes Using a $LiNO_3$-Gel Polymer Electrolyte, Monitored by Operando Neutron Depth Profiling

Liu, Ming; Cheng, Zhu; Qian, Kun; Verhallen, Tomas; Wang, Chao; Wagemaker, Marnix

DOI
10.1021/acs.chemmater.9b01325

Publication date
2019

Document Version
Final published version

Published in
Chemistry of Materials

CHEMISTRY OF MATERIALS
Cite This: Chem. Mater. 2019, 31, 4564−4574
Article
pubs.acs.org/cm

Efficient Li-Metal Plating/Stripping in Carbonate Electrolytes Using a $LiNO_3$-Gel Polymer Electrolyte, Monitored by Operando Neutron Depth Profiling

Ming Liu,[†,§] Zhu Cheng,[‡,§] Kun Qian,[†] Tomas Verhallen,[†] Chao Wang,[†] and Marnix Wagemaker*[,†]

[†]Section Storage of Electrochemical Energy, Radiation Science and Technology, Faculty of Applied Sciences, Delft University of Technology, 2629 JB Delft, Netherlands

[‡]Center of Energy Storage Materials & Technology, College of Engineering and Applied Sciences, National Laboratory of Solid State Microstructures, Collaborative Innovation Center of Advanced Microstructures, Nanjing University, Nanjing 210093, China

Supporting Information

ABSTRACT: The development of safe and high-performance Li-metal anodes is crucial to meet the demanded increase in energy density of batteries. However, severe reactivity of Li metal with typical electrolytes and dendrite formation leads to a poor cycle life and safety concerns. Therefore, it is essential to develop electrolytes that passivate the reactivity toward Li metal and suppress dendrite formation. Carbonate electrolytes display severe reactivity toward Li metal; however, they are preferred above the more volatile ether-based electrolytes. Here, a carbonate electrolyte gel polymer approach is combined with $LiNO_3$ as an additive to stabilize Li-metal plating. This electrolyte design strategy is systematically monitored by operando neutron depth profiling (NDP) to follow the evolution of the plated Li-metal density and the inactive lithium in the solid electrolyte interface (SEI) during cycling. Individually, the application of the $LiNO_3$ electrolyte additive and the gel polymer approach are shown to be effective. Moreover, when used in conjunction, the effects are complementary in increasing the plated Li density, reducing inactive Li species, and reducing the overpotentials. The $LiNO_3$ additive leads to more compact plating; however, it results in a significant buildup of inactive Li species in a double-layer SEI structure, which challenges the cell performance over longer cycling. In contrast, the gel polymer strongly suppresses the buildup of inactive Li species by immobilizing the carbonate electrolyte species; however, the plating is less dense and occurs with a significant overpotential. Combining the $LiNO_3$ additive with the gel polymer approach results in a thin and homogeneous SEI with a high conductivity through the presence of Li_3N and a limited buildup of inactive Li species over cycling. Through this approach, even high plating capacities, reaching 7 mAh/cm^2, can be maintained at a high efficiency. The rational design strategy, empowered by monitoring the Li-density evolution, demonstrates the possibilities of achieving stable operation of Li metal in carbonate-based electrolytes.

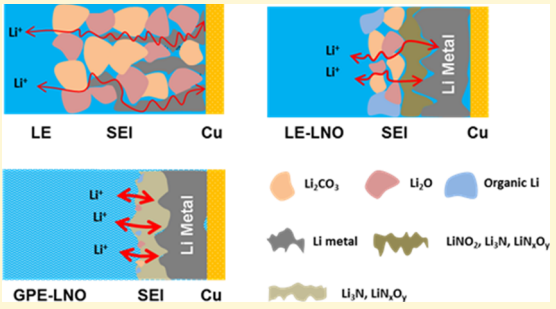

1. INTRODUCTION

In the past and present, intensive research has been and is devoted toward research and development of safe lithium (Li)-metal anodes.[1,2] From the perspective of energy density, Li metal is the ideal anode because of its high theoretical specific capacity of 3860 mAh g^{-1} and ultralow reduction potential properties (−3.040 V vs SHE) as compared to the traditional graphite-based anode.[3,4] However, the reactivity with typical carbonate electrolytes leads to severe capacity loss, resulting in a low Coulombic efficiency and poor cycle life.[5] In theory, during plating and when the current exceeds the Li-ion transport supported by the conductivity of the electrolyte, ion depletion at the Li-metal surface will occur after a characteristic time, which is referred to as Sand's time.[1,6] Under these conditions, plating becomes inhomogeneous, and self-amplified growth of dendrites is induced. The large surface area of dendrites exposes fresh electrolyte to the Li metal, which accelerates electrolyte decomposition. In practice, the inhomogeneous structure of the reduced liquid electrolyte (LE) species forming a solid electrolyte interface (SEI) promotes dendrite formation even at relatively low currents. Therefore, the formation of the SEI and Li-metal dendrites is a self-amplifying detrimental process, giving rise to severe irreversible capacity loss (including SEI formation and isolated "dead" Li metal). This increases the impedance, which lowers the cycling capacity and Coulombic efficiency and leads to early cell death.[7,8] Additionally, when Li-metal dendrites penetrate the separator and reach the cathode, an internal short circuit may lead to spontaneous discharge, which generates heat, potentially leading to a thermal runaway and the associated safety hazards.[1,6,9] For this reason, Li-metal anode research has moved largely from carbonates to ether-

Received: April 3, 2019
Revised: May 22, 2019
Published: May 23, 2019

DOI: 10.1021/acs.chemmater.9b01325
Chem. Mater. 2019, 31, 4564−4574

based electrolytes. Decomposition of the electrolytes leads to the formation of a flexible oligomeric SEI at the Li-metal surface, which significantly slows down electrolyte degradation.[3,10,11] However, ether-based electrolytes are more volatile and combustive and have a low oxidation potential (<4 V vs Li^+/Li), making these less safe, unsuitable to be combined with emerging high-voltage cathodes, and thus unsuitable for mass production.[12−14] Therefore, the search for strategies that allow the use of carbonate-based electrolytes, currently used in all commercial Li-ion batteries, in Li-metal batteries has become an important topic of research.[15] This research requires critical monitoring and understanding of the lithium-metal plating/stripping processes in realistic battery conditions.

It is well accepted that the Li metal reduces carbonate-based electrolytes, leading to the growth of mossy/dendritic lithium growing toward the separator, initiating further electrolyte decomposition.[16] Previous research has shown that the formation of lithium dendrites can be reduced in carbonated-based electrolytes by (1) utilizing polymer electrolytes, which immobilize the electrolyte species (including gel polymer electrolytes and solid polymer electrolytes),[17−21] (2) electrolyte additives to improve the SEI structure (such as fluoroethylene carbonate and $LiNO_3$),[15,22−27] and (3) introducing an artificial SEI on the current collector.[28−31] The core concepts include the promotion of Li-metal nucleation, homogenization of the Li flux, and reduction of the reactivity between electrolyte and fresh lithium by a favorable SEI structure and composition.[2] An important aspect is the optimization of electron and Li^+ transport through the Li metal and SEI layer, which directly affects the distribution of the Li ions and the Li-metal morphology.[32] Specifically, Zeng et al.[17] and Lu et al.[18] found that building the polymer matrix in carbonate-based electrolytes can promote uniform Li plating/stripping due to a lower resistance toward Li-ion diffusion, thus restricting the growth of dendritic and porous Li-metal morphologies. However, only surface morphologies observed by scanning electron microscopy (SEM) can be shown to support these results. Most recently, Shi et al.[10] found that adding $LiNO_3$ facilitates deep Li-metal cycling of 10 mAh cm^{-2} in ethylene carbonate/dimethyl carbonate (EC/DMC) electrolytes, renewing the possibilities for carbonated-based electrolytes. Furthermore, Liu et al.[15] discovered that nitrate anions in carbonate-based electrolytes dramatically alter the Li-metal nucleation, resulting in spherical metal nucleation and growth rather than dendritic growth, which were previously only observed for ether-based electrolytes. These results open up new directions for the application of carbonated-based electrolytes in lithium-metal batteries.

To gain more understanding of the underlying mechanisms of Li-metal plating and to push forward the development of Li-metal anodes, new electrolyte strategies would benefit from the ability to monitor its working conditions in operando. However, operando research toward the Li metal is challenging due the difficulty to detect Li, both its distribution and chemical form, in particular during battery operation.[1,9] Most techniques including microscopic and spectroscopic characterization methods may influence the electrochemistry and the lithium-metal anode itself.[31,33−37] Recently, Wang's group[38,39] and our group[40] introduced neutron depth profiling (NDP) as a powerful tool to monitor the average Li-metal density parallel to the current collector plane. NDP is isotope-specific and considered as a noninvasive and nondestructive technique. With this technique, the formation of inactive Li (in the SEI and as dead Li metal) and the Li-metal plating/stripping can be monitored quantitatively under operando conditions in liquid electrolytes.[40]

Here, NDP is used to monitor the lithium plating/stripping for different electrolytes. The $LiNO_3$ additive in EC/DMC carbonate-based electrolytes is shown to change the SEI formation and the Li-metal plating/stripping mechanism, which is responsible for the significant improvement in plating and stripping efficiency. However, at low current densities, the long exposure time of the electrolyte to the lithium metal results in a low efficiency. This continuously thickens the SEI film and results in accumulation of inactive lithium species, as observed by operando NDP. Based on these findings, the contact area between the electrolyte and lithium metal was reduced by introducing an acrylate-based gel polymer electrolyte (GPE). Although this was found to substantially reduce the formation of inactive Li, the relatively large overpotential indicates poor charge transport, introducing the conditions that promote dendrite formation. Combining the complementary and beneficial impact of the $LiNO_3$ additive and the GPE approach leads to a significant improvement in the Li-metal plating and stripping, minimizing the irreversible formation of inactive Li metal and strongly improves the electrochemical performance of the Li-metal anode.

2. METHODS

2.1. Preparation of Operando NDP Batteries and Electrochemical Tests. The schematic fabrication route of a pouch cell is shown in Figure S1. A pouch cell was fabricated with ∼11 μm-thick Cu foil (MTI Corporation, >99.99%), which functions as both the working electrode and as a window of the operando cell toward the NDP detector. The separator was a 300 μm glass fiber sheet (Whatman GF/D) loaded with or without $LiNO_3$ facing the lithium metal and a 25 μm PE (Celgard 2300) sheet facing the copper window. The $LiNO_3$-loaded glass fiber was prepared by soaking in 0.4 g of $LiNO_3$ and 10 mL of 1,2-dimethoxyethane (DME) solution for 2 h at room temperature. The soaked separators were then taken out of the solution and fully dried in an Ar-filled glove box overnight at room temperature. The mass loading of $LiNO_3$ on a separator was weighed to be ∼0.4 mg/cm^2. In total, 500 μL of conventional carbonate electrolyte (1 M $LiPF_6$ in 1:1 v/v EC/DMC, referred to as LE) or GPE precursor was added to the pristine or modified separator. The precursor solution was composed of 5 wt % TPGDA ($C_{15}H_{24}O_6$, MW = 300.35, Aldrich) monomer and 0.1 wt % AIBN ($C_8H_{12}N_4$, MW = 164.21, Aldrich) initiator dissolved in the LE. The cells with GPE were then heated at 60 °C for 6 h to ensure full polymerization of TPGDA in the LE.[41] The Li-metal foil (∼500 μm, Aldrich, 95 wt % ^{6}Li and 5 wt % ^{7}Li, density of 0.47 g cm^{-3}) serves as both the counter electrode and reference electrode. Galvanostatic cycling was performed by deposition of Li onto the Cu working electrode with different current densities up to a fixed capacity (1 to 7 mAh/cm^2), followed by Li stripping at different current densities up to 1 V.

2.2. NDP Experiments and Data Handling. Neutron depth profiling was performed on thermal neutron beamline A at the Reactor Institute Delft. Figure 1a shows the schematic setup of the operando NDP measurement. The ^{6}Li isotope undergoes a neutron capture reaction. This reaction between a neutron and the core of the atom produces two particles: $^4He^{2+}$ (E_k = 2044 keV) and $^3H^+$ (E_k = 2727 keV), emitted in all directions. As these particles travel through the sample, energy is lost due to interactions with the surrounding electron density. Due to the higher mass and valence state as well as their lower initial energy, the helium ions experience a larger stopping power than the hydrogen ions, which prevents them from reaching the detector in the present type of experiments.[42] The detector is placed at a distance of 4.5 cm from the pouch cells, and it detects the tritons ($^3H^+$) that leave the pouch cell perpendicular to the sample plane. The energy loss of the $^3H^+$ particles is measured with the

DOI: 10.1021/acs.chemmater.9b01325
Chem. Mater. 2019, 31, 4564−4574

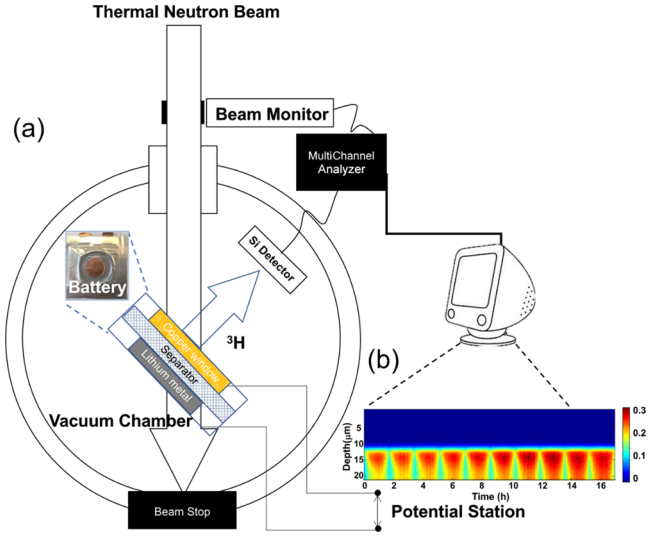

Figure 1. Principle of operando neutron depth profiling of Li-metal plating and stripping. (a) Schematic setup of operando neutron depth profiling of Li-metal plating and stripping. (b) Operando NDP measurements of 10 plating and stripping cycles at 1 mA cm^{-2} current density. The depth is measured from the outside surface of the copper; hence, the plating starts at ∼11 μm, representing the thickness of the copper-current collector window.

charged particle implanted Si detector (standard PIPs detector by Mirion Technologies, 1.1 × 1.1 cm^2) having a resolution of 14 keV. Based on the surface area of the detector, ∼2% of these tritons ($^3H^+$) reach the detector. The energy spectrum is processed by a multichannel analyzer (MCA, Canberra Industries, Spectrum Master) with 3.3 keV channels. Based on this setup, it is possible to monitor the Li density parallel to the electrode plane quantitatively in realistic battery geometries, as previously demonstrated in thin-film solid-state microbatteries,[43] Sn and Al electrodes,[44,45] $LiFePO_4$ electrodes,[46,47] and Li-metal plating at the interface of a garnet solid electrolyte.[38] The energy loss for the $^3H^+$ particles through the pouch cell material does not allow the measurement of the Li density inside the cell. Therefore, the pouch cell is modified by sealing it in the Cu-current collector of ∼11 μm in thickness, which allows us to probe ∼23 μm inside the cell. The counter electrode is a ^{6}Li-enriched Li metal (95% ^{6}Li and 5% ^{7}Li) that enhances the NDP signal intensity. The electrolyte in the pouch cell is 1 M $LiPF_6$ in EC/DMC (1:1), which was ^{6}Li-enriched by bringing it in contact with enriched lithium metal for 1 week by which the exchange current density equilibrates the ^{6}Li density toward 95%.

It should be mentioned that NDP is traditionally performed under high vacuum conditions. However, to enable electrochemically cycling of the pouch cells containing liquid electrolytes, the NDP measurements were performed under reduced air pressure (100 Torr N_2 equivalent), just above the vapor pressure of the electrolytes. This results in additional but marginal energy loss of the tritons and results in straggling on the air molecules, which compromises the energy resolution. One raw data profile from the operando measurements for the Li/GPE/Cu battery, with 3 min measurement time, is shown in Figure S2. The impact of straggling is demonstrated by the gradual increase in the measured $^3H^+$ intensity at the high energy (channel side), representing Li near the Cu-current collector.

To relate the triton ($^3H^+$) energy loss and intensity to the Li depth and Li density, the data needs to be corrected for the stopping power of the materials. The energy-dependent stopping power was calculated for the 11 μm copper-current collector (density of 8.96 g/cm^3) for the electrolyte based on 1 M $LiPF_6$ in 1:1 (v/v) EC/DMC, and for the ^{6}Li-enriched Li metal, the specified isotope ratio was used (95 wt % ^{6}Li and 5 wt % ^{7}Li, density of 0.47 g cm^{-3} using SRIM (2013 version)).[48] The detailed process of performing these corrections can be found in Figures S3 and S4 (Supporting Information).

The resolution in depth is determined by the energy resolution of the detector, the geometrical distribution in path lengths of the $^3H^+$ particles. Additionally, the low air pressure (100 Torr) leads to straggling of the $^3H^+$ particles, and hence, a distribution in energies also adds to the depth resolution. In combination with the distribution in thickness of the deposited Li metal, it is hard to quantitatively determine the depth resolution and, in particular, the changes in distributions. Integrated intensities provide insight into the processes.

It is important to realize that the neutron flux is small, ∼10^7 n/(cm^2·s), 10−20% of which is consumed by the capture reaction in the sample. As a consequence, the total amount of ^{6}Li consumed during the measurements is 1:10^{15} n/s, which is negligible. Therefore, NDP should be considered a nondestructive and noninvasive technique. In the present samples, only Al activates significantly due to the neutron beam. Al is present in the NDP chamber and has a significant cross section for thermal neutron capture (12 barn). It leads to β^- decay (4.6 MeV) with a half-life of 2.2 min, which yields ^{28}Si via prompt γ emission of a 1778 keV photon. Neutron capture of ^{63}Cu results in ^{64}Cu, which leads to β^- and β^+ decay, and ^{66}Cu to β^+ decay, with a half-life of 12.7 h and 5 min. Therefore, samples should be stored for ∼1 week before disposal.

2.3. SEM and XPS Characterization of the Materials and Electrodes. Lithium-metal-plating electrodes were prepared by discharging the pouch cell for 1 mAh/cm^2 capacity. Before SEM imaging, the electrodes were rinsed with dimethyl carbonate in a glove box under a dry argon atmosphere and dried several times in a vacuum chamber. Cross-section SEM samples were made by cutting the samples with a diamond saw in the glove box. Subsequently, samples were transferred into an SEM (JEOL JSM-6010LA) machine under dry argon conditions, and images were taken using an accelerating voltage of 10 kV (secondary electron).

An X-ray photoelectron spectrometer with Ar^+ beam was employed to investigate the element states in plated lithium on a copper foil (PHI5000 VersaProbe-II). Samples were placed on the XPS vacuum holder in the glove box and transferred to the XPS spectrometer to prevent moisture/air exposure. The applied X-ray source was monochromatic Kα X-rays at 1486.6 eV (aluminum anode) under ultrahigh vacuum (10^{-9} Torr) conditions. The instrument work function was calibrated to give a binding energy (BE) of 83.96 eV for the Au $4f_{7/2}$ line on a metallic gold reference sample, and the spectrometer dispersion was adjusted to give a BE of 932.62 eV for the Cu $2p_{3/2}$ line on a metallic copper sample. The depth-profiling sputtering was conducted by 1 min sputtering in five cycles (2 kV, 2 × 2 mm) and followed by 8 min sputtering in 10 cycles (2 kV, 2 × 2 mm); the narrow spectra of particular elements (Li, O, and N) were recorded after each cycle of sputtering. The pass energy used for the hemispheric analyzer was 58.7 eV, and the base pressure of the system was ∼1 × 10^{-7} Pa. The estimated sputtering rates are 6 nm/min.

3. RESULTS AND DISCUSSION

3.1. Operando NDP Measurement of the Lithium Stripping/Plating in the Liquid Electrolyte (LE), the LE with the $LiNO_3$ Additive, and the Gel Polymer Electrolyte (GPE). In Figure 1b, the results of operando NDP are shown for 10 subsequent electrochemical plating and stripping cycles at 1 mA/cm^2 up to a plating capacity of 1 mAh/cm^2, during which continuous 3 min NDP measurements were acquired. The Li signal upon Li-metal plating appears at a depth of 11 μm on the copper-current collector window facing the electrolyte. As can be anticipated, the Li signal increases up to the end of discharge and decreases upon subsequent stripping. The depth resolution for these systems is ∼0.1 μm, which is dictated by the stopping power of the materials along the path of the $^3H^+$ between the Li position, straggling, and the detector resolution.[40] Note that the signal is averaged over an

DOI: 10.1021/acs.chemmater.9b01325
Chem. Mater. 2019, 31, 4564−4574

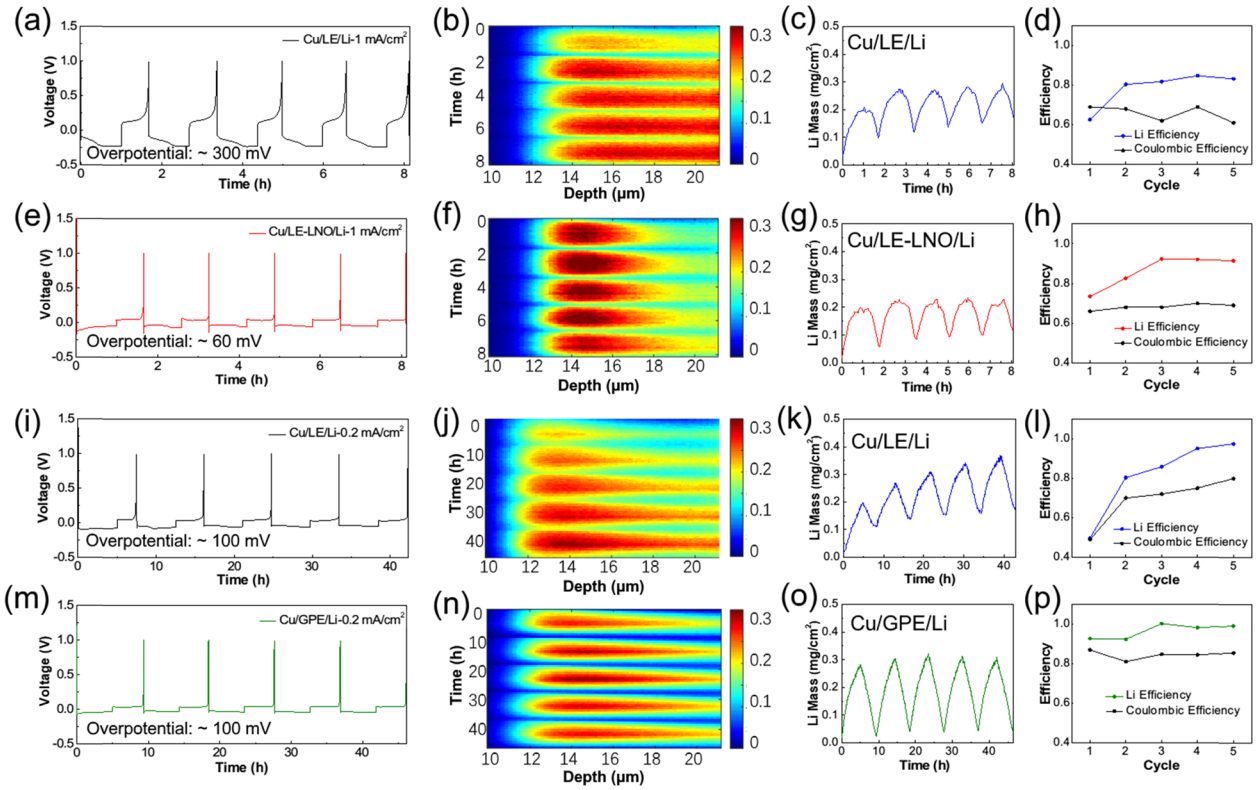

Figure 2. Impact of the $LiNO_3$ additive in the LE and GPE on the Li-density depth distribution. (a–d) Electrochemical performance, Li distribution, Li mass, and Li efficiency from operando NDP of the Cu/LE/Li batteries for five plating/stripping cycles at 1 mA/cm^2. (e–h) Electrochemical performance, Li distribution, Li mass, and Li efficiency from operando NDP of the Cu/LE-LNO/Li batteries for five plating/stripping cycles at 1 mA/cm^2. (i–l) Electrochemical performance, Li distribution, Li mass, and Li efficiency from operando NDP of the Cu/LE/Li batteries for five plating/stripping cycles at 0.2 mA/cm^2. (m–p) Electrochemical performance, Li distribution, Li mass, and Li efficiency from operando NDP of the Cu/GPE/Li batteries for five plating/stripping cycles at 0.2 mA/cm^2. The depth is measured from the outside surface of the copper; hence, the plating starts at ~11 μm, representing the thickness of the copper-current collector window. The color scale of the NDP measurements indicates the fractional Li density normalized to the Li metal.

~1 cm^2 electrode. The Li density is normalized to the Li metal. Hence, it reflects the fractional density with respect to the Li metal.[40] Figure 1b demonstrates the instability of the EC/DMC electrolyte as the Li density progressively increases irreversibly both in intensity and depth, indicating the buildup of inactive Li and growing porous structures, as further testified by Figure S5.

Utilizing $LiNO_3$ as an SEI-forming agent is widely adopted for ether-based electrolytes and has recently been shown also to efficiently passivate the lithium surface and positively affect the SEI composition in carbonated-based electrolytes.[10,15] At present, the role of $LiNO_3$ in the LE (LE-LNO) toward the lithium stripping/plating was investigated by operando NDP, the results of which are shown in Figure 2a–h. As the solubility of $LiNO_3$ in carbonate-based electrolytes is low, the $LiNO_3$ was loaded on the glass fiber separator, leading to a slow release of $LiNO_3$ in the electrolyte as it is consumed by the SEI formation.[10] Comparing the first five cycles at 1 mA/cm^2 with and without the $LiNO_3$ additive shows marked differences in the overpotential and plated lithium depth. As shown in Figure 2a,e, adding $LiNO_3$ results in a significant drop in overpotential from ~300 to ~100 mV. Interestingly, the $LiNO_3$ additive leads to a much more compact and, hence, dense plating, as demonstrated in Figure 2e,f. Li-metal plating in the pure LE results in a porous Li morphology with low-density tails extending deep into the electrolyte already after two cycles (Figure 2b), which reflects the EC/DMC electrolyte reduction that leads to low-density lithium-metal plating.[49,50] It should be realized that the total amount of inactive Li quantified by NDP is a combination of dead Li metal and inactive Li in the SEI as the chemical nature of Li cannot be distinguished by NDP.[40] Consistently, postmortem SEM shows that the thickness of the lithium anode after discharge in the battery with the $LiNO_3$ additive was only ~7.8 μm (Figure S5c). For the pure LE, SEM in Figure S5a,b shows a rough, porous morphology representing mossy lithium growth as a consequence of the high reactivity between the fresh Li metal and LE. Figure S5d shows the surface morphology of the lithium deposition in the presence of the $LiNO_3$ additive, which displays more uniform plating and larger lithium metal particles.

Figure 2c,g represents the evolution of the lithium mass during five cycles, which is determined by integrating the NDP spectra over the complete depth at each time during cycling. The ability of NDP to monitor the amount of Li metal on the current collector allows us to determine the Li efficiency, defined as the ratio of the stripped with the plated amount of Li within the maximum depth probed by the NDP. Therefore, it provides complementary information to the electron efficiency as quantified by the Coulombic efficiency.[40] The difference between the Coulombic efficiency and Li efficiency quantifies the amount of irreversible reactions that do not involve Li-ion transfer, such as direct electrolyte reduction and chemical dissolution of Li from the SEI. Chemical dissolution does not appear to play a role as, during a relaxation

DOI: 10.1021/acs.chemmater.9b01325
Chem. Mater. 2019, 31, 4564–4574

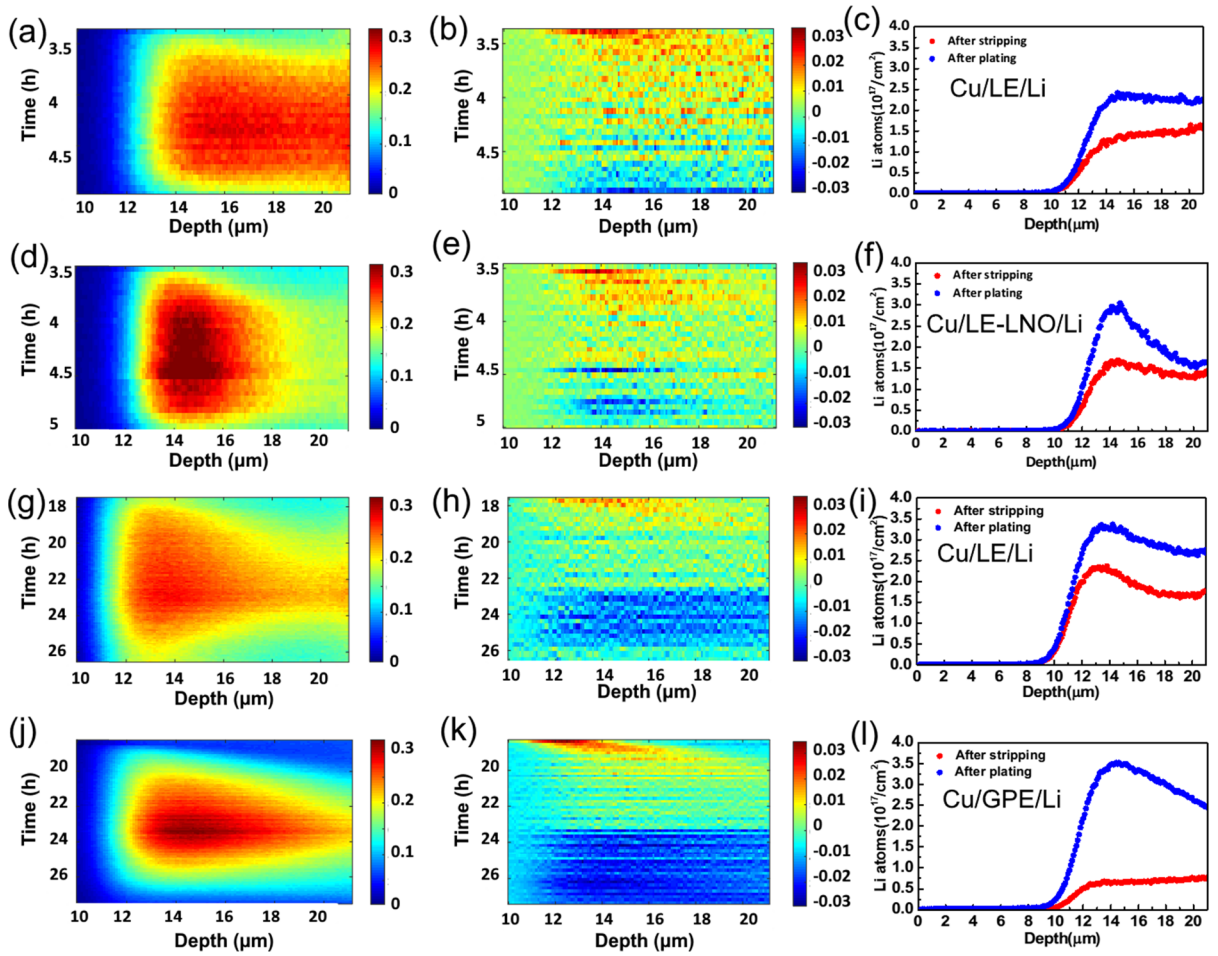

Figure 3. Impact of $LiNO_3$ and the GPE on the Li-density depth distribution. (a–c) Operando NDP measurements of the third plating and stripping cycle of the Cu/LE/Li battery including the plating and stripping activity and Li density at 1 mA/cm^2. (d–f) Operando NDP measurements of the third plating and stripping cycle of the Cu/LE-LNO/Li battery including the plating and stripping activity and Li density at 1 mA/cm^2. (g–i) Operando NDP measurements of the third plating and stripping cycle of the Cu/LE/Li battery including the plating and stripping activity and Li density at 0.2 mA/cm^2. (j–l) Operando NDP measurements of the third plating and stripping cycle of the Cu/GPE/Li battery including the plating and stripping activity and Li density at 0.2 mA/cm^2. The depth is measured from the outside surface of the copper; hence, the plating starts at ∼11 μm, representing the thickness of the copper-current collector window. The color scale of the NDP measurements indicates the fractional Li density normalized to the Li metal.

experiment, no change in the Li-density profile was observed (see Figure S6). The Li efficiency and Coulombic efficiency for the LE and LE-LNO electrolytes are shown in Figure 2d,h. Clearly, a low Li efficiency, associated with the high reactivity, results in a rapid accumulation of dead lithium during cycling despite the presence of the $LiNO_3$ additive. In summary, the Cu/LE/Li and Cu/LE-LNO/Li batteries show, not unexpectedly, dead lithium accumulation and a relative low efficiency, whereas the LNO additive is demonstrated to result in a more compact plating.

Previously, it has been demonstrated that the use of a GPE enhances the performance of lithium metal batteries.[17−21] Here, operando NDP is also performed to understand the origin of this improvement. For this experiment, a tri-(propylene glycol) diacrylate (TPGDA)-based GPE is used. TPGDA is a typical acrylate-based monomer that polymerizes in situ in the LE, thereby immobilizing the LE and decreasing the reactivity of the electrolyte, as demonstrated by our previous work.[41] A comparison of the Li-density evolution between the LE and GPE is shown in Figure 2i–p. Clearly, the plated lithium for the GPE is almost completely stripped, and consequentially, much less inactive lithium accumulates upon cycling. Figure 2k,o shows the integrated amount of Li on the current collectors, demonstrating a higher Li efficiency and better reversibility of the GPE compared to the LE.

In Figure 2l,p, the Coulombic efficiency is shown as determined from the galvanostatic cycling next to the Li efficiency obtained from the NDP measurements. The Cu/GPE/Li demonstrates higher Coulombic and Li efficiencies, indicating that the GPE can largely alleviate the consumption of the plated lithium metal by side reactions with the electrolyte. For the Cu/LE/Li cell, the low initial Li efficiency results in an accumulation of inactive lithium species, including Li_2O, Li_2CO_3, and isolated Li metal, forming a mosaic structure covering the Cu-current collector.[51] This SEI is the origin of the overpotential increase, and the heterogeneous SEI structure is believed to promote dendrite formation, introducing fresh electrolyte-Li metal contact, a self-amplifying process that results in rapid battery failure. The postmortem SEM images of the plated Li metal morphology, at a current density of 0.2 mA/cm^2 to a capacity of 1 mAh/cm^2, are shown in Figure S5e,f. For the LE, the images show a porous and

DOI: 10.1021/acs.chemmater.9b01325
Chem. Mater. 2019, 31, 4564−4574

mossy surface after plating. In contrast, the GPE shows a relatively dense Li metal/SEI morphology. This can be rationalized by the reduced mobility of the LE, preventing side reactions between the LE and fresh lithium metal.

Figure 3a,d compares the Li density during the third cycle in the LE-based battery with and without the $LiNO_3$ additive, again demonstrating the more dense and compact plating due to the presence of the $LiNO_3$ additive. The activity in Figure 3b,e is obtained by taking the difference of two subsequent measurements for each time step (each taking 10 min), thus representing lithium plating/stripping activity during each 10 min. This provides direct insight into the distribution of the plating and stripping, resulting in a positive change in Li density during plating (yellow/red) and a negative change in Li density during stripping (blue). The plating and stripping activity indicates that, in the early stages of the plating, Li is more compact with the presence of $LiNO_3$. In the second stage, the Li density increases more homogeneously, most likely induced by electrolyte decomposition. This is supported by Figure 3f, showing a large amount of inactive Li left after stripping. For the regular electrolyte, the homogeneous increase in Li density appears to start at an even earlier stage. Consequently, the amount of inactive Li due to electrolyte reduction after stripping is also larger, as is shown in Figure 3c. Even though the porous dendritic structures are known to grow from the interface with the Cu-current collector, the activity is observed at the electrolyte side as the porous structure is pushed into the electrolyte.

Plating the Cu/LE/Li cell at a lower current density, shown in Figure 3g–i, results in a less dense layer that extends beyond the maximum depth that can be probed by NDP. This more porous morphology is a direct result of the longer contact time between the Li metal and LE during slower cycling. This confirms that there is a strong relationship between the reactivity of the electrolyte and the resulting Li-metal density profile. Although the $LiNO_3$ additive leads to a more compact plating and lower plating and stripping overpotentials, it does not prevent severe electrolyte decomposition responsible for the observed high inactive Li density. The aim of introducing the GPE is to diminish the buildup of inactive Li species by reducing the contact area with the electrolyte and by demobilizing the electrolyte solvent species. As shown in Figure 3j, the very low lithium concentration at the beginning and at the end of the third cycle of the Cu/GPE/Li battery reveals that the GPE indeed largely prevents the formation of inactive Li species. From the plating/stripping activity of the Cu/GPE/Li, Figure 3k, it can be concluded that Li nucleation occurs close to the interface with the copper foil. Although the plating appears to be less dense compared to the LE with the $LiNO_3$ additive, the stripping is more efficient, as demonstrated by Figure 3l. Despite the higher Li efficiency at 1 mA/cm^2, the Cu/GPE/Li cell displays a relatively high overpotential (~200 mV) compared to the Cu/LE-LNO/Li cell (~100 mV), as shown in Figure S7. The high overpotential results in a low voltage efficiency and could, upon extended cycling, lead to enhancement of decomposition reactions. Hence, the origin of the improved plating/stripping appears to be fundamentally different for the LE-LNO and GPE electrolytes. For the $LiNO_3$ additive in the carbonate LE, a low overpotential and compact plating are achieved, whereas the GPE provides a high Li efficiency. This indicates that integrating the GPE with the $LiNO_3$ additive may be a promising strategy toward improved Li-metal anode performance.

3.2. Operando NDP Measurement of the Lithium Stripping/Plating in the Gel Polymer Electrolyte with the $LiNO_3$ Additive (GPE-LNO).

The galvanostatic cycling toward different capacities of the GPE including the $LiNO_3$ additive, referred to as the Cu/GPE-LNO/Li battery, is shown in Figure 4. The battery displays an overpotential of ~120 mV

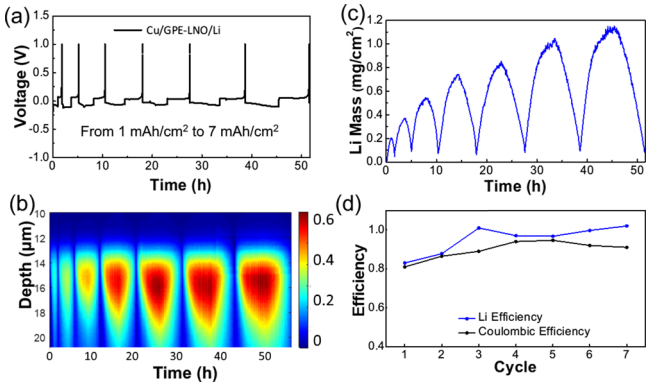

Figure 4. Impact of the GPE and $LiNO_3$ combination on the Li-density distribution. (a–d) Electrochemical performance, Li distribution, Li mass, and Li efficiency from operando NDP of the Cu/GPE-LNO/Li battery at 1 mA/cm^2 for 1 to 7 h. The depth is measured from the outside surface of the copper; hence, the plating starts at ~11 μm, representing the thickness of the copper-current collector window. The color scale of the NDP measurements indicates the fractional Li density normalized to the Li metal.

under 1 mA/cm^2 cycling, which is significantly lower than the GPE electrolyte, indicating the positive impact of the presence of the $LiNO_3$ additive (Figure 4a). Operando NDP in Figure 4b discloses that the Li-metal plating remains dense at a capacity of 1 mAh/cm^2. Cycling to 1 mAh/cm^2 (equivalent to a pure Li-metal film thickness of ~5 μm) results in an ~8 μm thickness of the plated morphology, which is very dense for a carbonate-based electrolyte.[52] In most research studies, Li-metal electrodes are generally plated up to relatively small capacities, that is, 1 mAh/cm^2; however, this is insufficient to achieve practical energy densities.[10] For instance, Li–S batteries for next-generation electric vehicles[53,54] require a sulfur cathode with a mass loading of 5 mg/cm^2 (~1000 mAh/g), which demands a lithium-metal capacity of at least 5 mAh/cm^2. From this practical perspective, the present Cu/GPE-LNO/Li battery is cycled up to capacities reaching 7 mAh/cm^2 at 1 mA/cm^2, as shown in Figure 4a. Even at a relatively large capacity of 7 mAh/cm^2, the GPE-LNO electrolyte results in compact plating at the Cu-current collector (Figure 4b), further indicating that the present electrolyte strategy is promising toward a stable Li-metal plating in carbonate-based electrolytes. Comparing the buildup of inactive Li in Figure 4c,d with that in Figure 2 for the LNO and GPE electrolytes demonstrates that even 7 mAh/cm^2 can be cycled with a relatively good reversibility. Clearly, the GPE component retains the ability to suppress the accumulation of inactive Li species. Note that, at large plating capacities, a part of the Li density falls outside the NDP detection range. In the NDP measurement, only the Li deposits within the detection limit, close to 23 μm for these measurements, can be determined. As a consequence, the Li efficiency and total plated mass can only accurately be determined if the Li density falls within the

DOI: 10.1021/acs.chemmater.9b01325
Chem. Mater. 2019, 31, 4564–4574

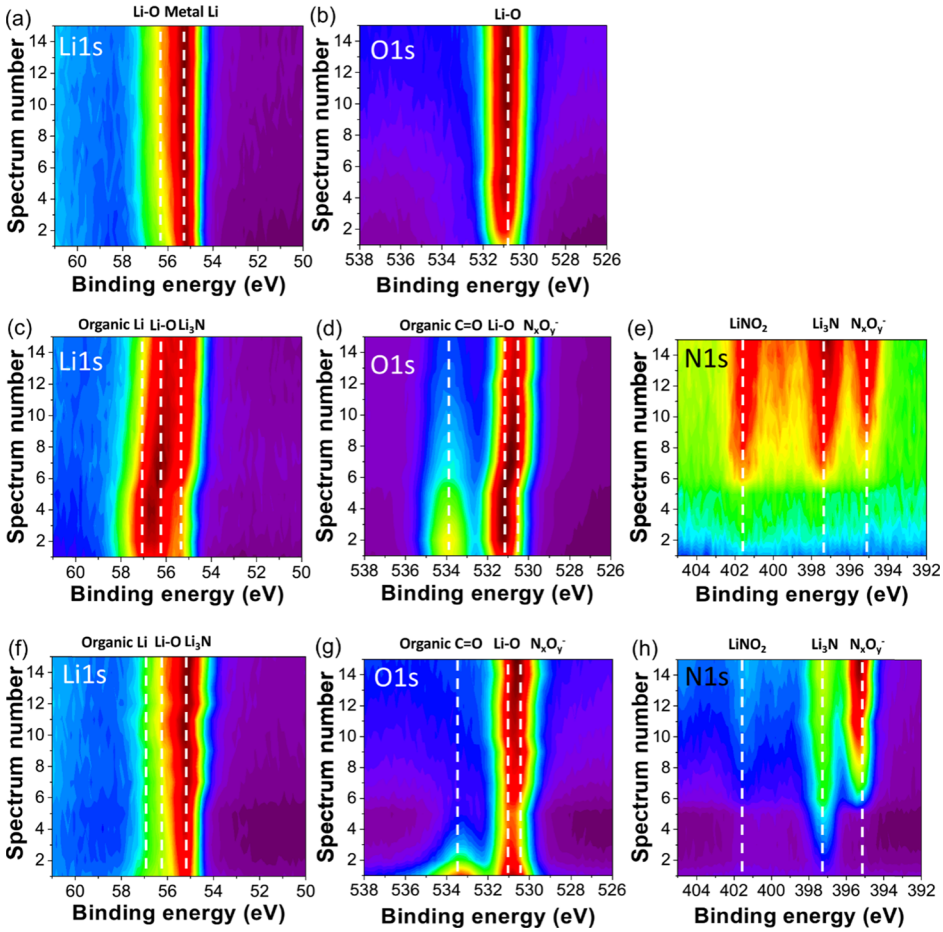

Figure 5. Chemical composition of the SEI from XPS. Li 1s, O 1s, and N 1s XPS depth profiles of cycled electrodes from (a, b) Cu/LE/Li, (c–e) Cu/LE-LNO/Li, and (f–h) Cu/GPE-LNO/Li batteries.

maximum depth observed. Specifically, this means that the results from Figure 2b are inaccurate from the first cycle, whereas it becomes inaccurate in Figure 2j after the second cycle. We estimate that, in Figure 4, the error in the Li efficiency is less than 5% as the intensity of the tail that is not completely observed is already far below that in the observed signal. The NDP results indicate that the Cu/GPE-LNO/Li battery cycles are relatively stable, as compared to the GPE and the LNO additive individually, at high areal capacities as demanded by practical applications.

Because NDP does not allow differentiation of the chemical Li species present in the different electrolyte systems, XPS depth profiling was performed under ex situ conditions after 1 mAh/cm^2 Li plating. The depth XPS profiles of Li 1s, O 1s, and N 1s of the LE, LE-LNO, and GPE-LNO cells are shown in Figure 5a–h. For the EC/DMC electrolyte, XPS in Figure 5a,b indicates the presence of mainly Li_2O/Li_2CO_3 in the SEI, as should be expected in carbonate electrolytes.[55−58] Note that Li_2CO_3 leads to nearly the same O 1s XPS energy compared to Li_2O, making this difficult to distinguish. The poor ionic conductivity of the mosaic SEI structure composed of Li_2O/Li_2CO_3 will hinder Li-ion transport and promote dendrite formation, which can be expected to be responsible for the large amount of inactive Li species[59,60] observed directly with NDP in Figure 4. Addition of $LiNO_3$ results in a very different SEI composition (see Figure 5c–e), introducing reduced $LiNO_3$ species such as Li_3N, $LiNO_2$, and LiN_xO_y, an observation in line with previous findings.[10,15] As Li_3N is an excellent Li-ion conductor (10^{-4} S/cm),[61] it can be held responsible for the lower overpotentials during plating and stripping (see Figure 3b). Interestingly, the SEI in the presence of $LiNO_3$ in the electrolyte appears to have a double-layer structure at the current collector composed of the reduced $LiNO_2$ species and, at the top, Li_2O/Li_2CO_3 and reduced electrolyte (ROLi) species. The latter testifies the remaining reactivity toward the electrolyte where, specifically, the ROLi species can be expected to be the result of EC reduction by the Li metal.[6,57,62] In contrast, as shown in Figure 5f–h, when combining the GPE and $LiNO_3$ additive, this results in a more uniform SEI with significantly less Li_2O/Li_2CO_3 and ROLi species. Therefore, in this case, the SEI can be expected to have the largest conductivity and contain less inactive Li components, consistent with the lower Li density left after stripping observed by the NDP results in Figure 4. The absence of the $LiNO_2$ species in the SEI formed in contact with the GPE-LNO electrolyte (see Figure 5h) may be explained by the better SEI conductivity, allowing further reduction of the $LiNO_3$ additive.[23,63,64] An interesting finding is that introduction of the $LiNO_3$ additive leads to the presence of organic species that contains C═O (Figure 5b,d,g), most likely the result of EC reduction by the Li metal, which is believed to play a major role in constituting a protective and passive film on the lithium anode.[65] Because traces of water should react with $(CH_2OCO_2Li)_2$ toward Li_2CO_3 and $(CH_2OH)_2$,[6] we speculate that the hygroscopic nature of the $LiNO_2$ species may be responsible for preventing this last

DOI: 10.1021/acs.chemmater.9b01325
Chem. Mater. 2019, 31, 4564−4574

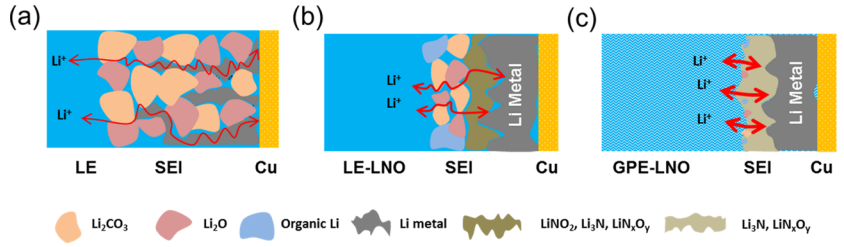

Figure 6. Schematic representations of the plating and stripping process for the different electrolytes. (a–c) Schematic representation of the plating and stripping process in LE, LE-LNO, and GPE-LNO electrolytes based on the operando NDP and XPS results.

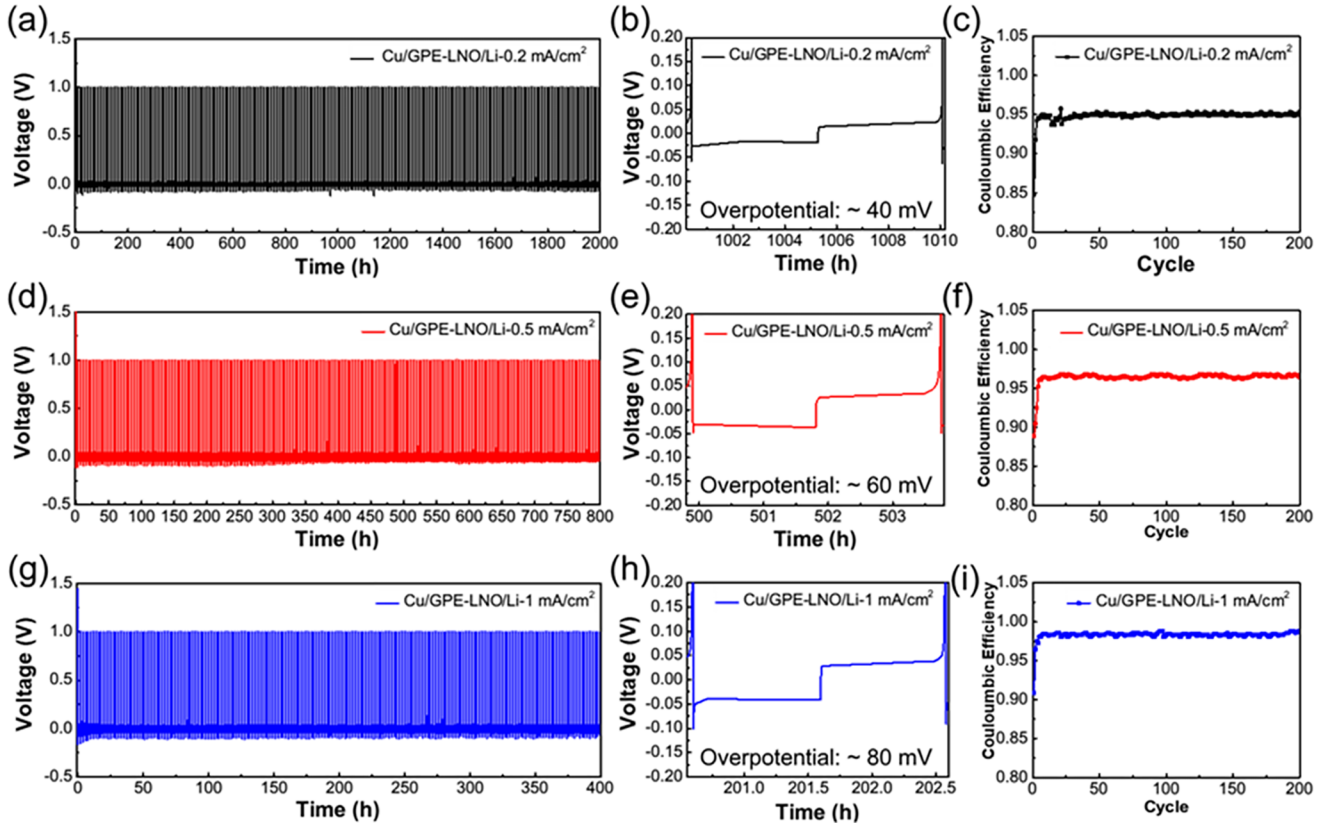

Figure 7. Electrochemical performance of the Cu/GPE-LNO/Li battery. (a–c) 0.2 mA/cm^2, (d–f) 0.5 mA/cm^2, and (g–i) 1 mA/cm^2.

reaction step. This demonstrates the complexity of the SEI reactions upon the introduction of additives.

Figure 6a–c shows schematic representations of the plating and stripping process based on the results of the operando NDP and the ex situ XPS and SEM experiments. In the EC/DMC carbonate electrolyte, NDP and SEM indicate increasingly porous plated Li morphologies upon cycling and the formation of a thick SEI layer with a large amount of inactive Li species. Moreover, XPS demonstrates that the main SEI constituents are the poorly conducting Li_2O/Li_2CO_3 species, explaining the large overpotential during cycling. Furthermore, this poorly conducting heterogeneous SEI will further enhance mossy/dendrite Li-metal formation and electrolyte degradation. Instead, reduction of the $LiNO_3$ additive leads to an SEI that is rich in $LiNO_2$, Li_3N, and LiN_xO_y species. The Li_3N component will enhance the ionic conductivity, responsible for the more compact plating and a lowering of the overpotential observed by NDP and SEM. However, the high reactivity between the Li metal and EC/DMC creates a heterogeneous top layer composed of Li_2O/Li_2CO_3 and reduced EC species that compromises the SEI conductivity. In addition, it leads to the development of a large amount of inactive Li, as observed by NDP. This is responsible for the relatively low plating and stripping efficiency and, upon long cycling, enhanced dendrite formation and electrolyte decomposition. Combining the GPE with the $LiNO_3$ additive leads to a further improved SEI morphology and composition, which is shown to be more compact and thinner as indicated by NDP and SEM, and is demonstrated to be more uniformly composed of Li_3N and LiN_xO_y, as shown by XPS. As a result, the conductivity can be expected to be high, which, in combination with a reduced buildup of inactive Li species over cycling, rationalizes the relatively good Li-metal anode performance of this carbonate-based electrolyte.

Finally, the GPE-$LiNO_3$ electrolyte cells were subjected to 200 cycles at 1 mAh/cm^2 at different current densities (0.2, 0.5, and 1 mA/cm^2). As shown in Figure 7a,d,g, this battery displays stable cycling and small overpotential values of 40, 60, and 80 mV for 0.2, 0.5, and 1 mA/cm^2, respectively (Figure 7b,e,h). Efficiencies of the battery, as shown in Figure 7c,f,i,

DOI: 10.1021/acs.chemmater.9b01325
Chem. Mater. 2019, 31, 4564–4574

maintain high values for carbonate electrolytes reaching ~95, 96, and 98% under 0.2, 0.5, and 1 mA/cm^2, respectively. The long-term stability, high efficiency, and low overpotential reflect the favorable SEI properties through the synergistic effect of the $LiNO_3$ additive and GPE electrolyte.

4. CONCLUSIONS AND OUTLOOK

To conclude, we have successfully developed an improved electrolyte design combining a carbonate-based gel polymer electrolyte and $LiNO_3$ as the additive, guided by monitoring of the Li-metal plating and stripping directly by operando NDP. The electrolyte composition has a dramatic effect on the evolution of the plated Li-density profile, where $LiNO_3$ as the additive to the carbonate electrolyte results in a more dense plating and favorable SEI composition. The remaining reduction of electrolyte species results in a nonuniform SEI layer that promotes the development of inactive Li over cycling. The GPE immobilizes the carbonate electrolyte species, largely preventing electrolyte reduction and, in combination with $LiNO_3$, forming a homogeneous good conducting SEI that suppresses porous/dendritic Li-metal plating. It should be realized that these electrolytes are not optimized, and further carbonate-based electrolyte development and optimization are likely to result in further improvement of the plating/stripping in efficiency, indicating the potential of the present strategy toward improved carbonate electrolytes for Li-metal batteries.

■ ASSOCIATED CONTENT

Supporting Information

The Supporting Information is available free of charge on the ACS Publications website at DOI: 10.1021/acs.chemmater.9b01325.

Fabrication method of the Cu/LE/Li, Cu/LE-LNO/Li, and Cu/GPE-LNO/Li batteries; SEM measurement showing the Li-plated metal morphology for the LE, LE-LNO, and GEO; electrochemical performance of the Cu/GPE/Li batteries working at 1 mA/cm^2; uncorrected NDP measurements, NDP correction methodology, and a NDP relaxation experiment (PDF)

■ AUTHOR INFORMATION

Corresponding Author

*E-mail: m.wagemaker@tudelft.nl.

ORCID

Marnix Wagemaker: 0000-0003-3851-1044

Author Contributions

§M.L. and Z.C. contributed equally to this work.

Notes

The authors declare no competing financial interest.

■ ACKNOWLEDGMENTS

The authors thank Michel Steenvoorden and Frans Ooms for their assistance with experiments. M.L. acknowledges the support by the Netherlands Organization for Scientific Research (NWO) under the grant no. 15788, and M.W. acknowledges the support under the VICI grant no. 16122. Financial support from the Advanced Dutch Energy Materials (ADEM) program of the Dutch Ministry of Economic Affairs, Agriculture and Innovation is gratefully acknowledged. We would like to thank the Chinese Scholarship Council (CSC) for financially supporting a part of the work in this paper.

■ REFERENCES

(1) Cheng, X.-B.; Zhang, R.; Zhao, C. Z.; Zhang, Q. Toward Safe Lithium Metal Anode in Rechargeable Batteries: A Review. *Chem. Rev.* **2017**, 10403.

(2) Lin, D.; Liu, Y.; Cui, Y. Reviving the lithium metal anode for high-energy batteries. *Nat. Nanotechnol.* **2017**, *12*, 194.

(3) Xu, W.; Wang, J.; Ding, F.; Chen, X.; Nasybulin, E.; Zhang, Y.; Zhang, J.-G. Lithium metal anodes for rechargeable batteries. *Energy Environ. Sci.* **2014**, *7*, 513.

(4) Liu, M.; Qin, X.; He, Y.-B.; Li, B.; Kang, F. Recent innovative configurations in high-energy lithium−sulfur batteries. *J. Mater. Chem. A* **2017**, *5*, 5222.

(5) Liu, F.-Q.; Wang, W.-P.; Yin, Y.-X.; Zhang, S.-F.; Shi, J.-L.; Wang, L.; Zhang, X.-D.; Zheng, Y.; Zhou, J.-J.; Li, L.; Guo, Y.-G. Upgrading traditional liquid electrolyte via in situ gelation for future lithium metal batteries. *Sci. Adv.* **2018**, *4*, eaat5383.

(6) Aurbach, D.; Zinigrad, E.; Cohen, Y.; Teller, H. A short review of failure mechanisms of lithium metal and lithiated graphite anodes in liquid electrolyte solutions. *Solid State Ionics* **2002**, *148*, 405.

(7) Chen, K.-H.; Wood, K. N.; Kazyak, E.; LePage, W. S.; Davis, A. L.; Sanchez, A. J.; Dasgupta, N. P. Dead lithium: mass transport effects on voltage, capacity, and failure of lithium metal anodes. *J. Mater. Chem. A* **2017**, *5*, 11671.

(8) Suo, L.; Hu, Y.-S.; Li, H.; Armand, M.; Chen, L. A new class of solvent-in-salt electrolyte for high-energy rechargeable metallic lithium batteries. *Nat. Commun.* **2013**, *4*, 1481.

(9) Zhang, R.; Li, N.-W.; Cheng, X.-B.; Yin, Y.-X.; Zhang, Q.; Guo, Y.-G. Advanced micro/nanostructures for lithium metal anodes. *Adv. Sci.* **2017**, *4*, 1600445.

(10) Shi, Q.; Zhong, Y.; Wu, M.; Wang, H.; Wang, H. High-capacity rechargeable batteries based on deeply cyclable lithium metal anodes. *Proc. Natl. Acad. Sci. U. S. A.* **2018**, *115*, 5676.

(11) Aurbach, D.; Youngman, O.; Gofer, Y.; Meitav, A. The electrochemical behaviour of 1, 3-dioxolane-$LiClO_4$ solutions-I. Uncontaminated solutions. *Electrochim. Acta* **1990**, *35*, 625.

(12) Xu, K. Nonaqueous liquid electrolytes for lithium-based rechargeable batteries. *Chem. Rev.* **2004**, *104*, 4303.

(13) Liu, M.; Zhou, D.; Jiang, H. R.; Ren, Y. X.; Kang, F. Y.; Zhao, T. S. A Highly-safe Lithium-ion Sulfur Polymer Battery with SnO_2 Anode and Acrylate-based Gel Polymer Electrolyte. *Nano Energy* **2016**, *28*, 97.

(14) Yan, C.; Yao, Y.-X.; Chen, X.; Cheng, X.-B.; Zhang, X.-Q.; Huang, J.-Q.; Zhang, Q. Lithium Nitrate Solvation Chemistry in Carbonate Electrolyte Sustains High-Voltage Lithium Metal Batteries. *Angew. Chem.* **2018**, *130*, 14251.

(15) Liu, Y.; Lin, D.; Li, Y.; Chen, G.; Pei, A.; Nix, O.; Li, Y.; Cui, Y. Solubility-mediated sustained release enabling nitrate additive in carbonate electrolytes for stable lithium metal anode. *Nat. Commun.* **2018**, *9*, 3656.

(16) Bai, P.; Li, J.; Brushett, F. R.; Bazant, M. Z. Transition of lithium growth mechanisms in liquid electrolytes. *Energy Environ. Sci.* **2016**, *9*, 3221.

(17) Zeng, X.-X.; Yin, Y.-X.; Li, N.-W.; Du, W.-C.; Guo, Y.-G.; Wan, L.-J. Reshaping lithium plating/stripping behavior via bifunctional polymer electrolyte for room-temperature solid Li metal batteries. *J. Am. Chem. Soc.* **2016**, *138*, 15825.

(18) Lu, Q.; He, Y.-B.; Yu, Q.; Li, B.; Kaneti, Y. V.; Yao, Y.; Kang, F.; Yang, Q.-H. Dendrite-Free, High-Rate, Long-Life Lithium Metal Batteries with a 3D Cross-Linked Network Polymer Electrolyte. *Adv. Mater.* **2017**, *29*, 1604460.

(19) Zhou, W.; Wang, S.; Li, Y.; Xin, S.; Manthiram, A.; Goodenough, J. B. Plating a dendrite-free lithium anode with a polymer/ceramic/polymer sandwich electrolyte. *J. Am. Chem. Soc.* **2016**, *138*, 9385.

(20) Khurana, R.; Schaefer, J. L.; Archer, L. A.; Coates, G. W. Suppression of lithium dendrite growth using cross-linked poly-

DOI: 10.1021/acs.chemmater.9b01325
Chem. Mater. 2019, 31, 4564−4574

ethylene/poly (ethylene oxide) electrolytes: A new approach for practical lithium-metal polymer batteries. *J. Am. Chem. Soc.* **2014**, *136*, 7395.
(21) Liu, M.; Zhou, D.; He, Y.-B.; Fu, Y.; Qin, X.; Miao, C.; Du, H.; Li, B.; Yang, Q.-H.; Lin, Z.; Zhao, T. S.; Kang, F. Novel gel polymer electrolyte for high-performance lithium−sulfur batteries. *Nano Energy* **2016**, *22*, 278.
(22) Zhang, T.; Liao, K.; He, P.; Zhou, H. A self-defense redox mediator for efficient lithium−O_2 batteries. *Energy Environ. Sci.* **2016**, *9*, 1024.
(23) Rosenman, A.; Elazari, R.; Salitra, G.; Markevich, E.; Aurbach, D.; Garsuch, A. The Effect of Interactions and Reduction Products of $LiNO_3$, the Anti-Shuttle Agent, in Li-S Battery Systems. *J. Electrochem. Soc.* **2015**, *162*, A470.
(24) Jozwiuk, A.; Berkes, B. B.; Weiß, T.; Sommer, H.; Janek, J.; Brezesinski, T. The critical role of lithium nitrate in the gas evolution of lithium-sulfur batteries. *Energy Environ. Sci.* **2016**, *9*, 2603.
(25) Zhang, S. S. Role of $LiNO_3$ in rechargeable lithium/sulfur battery. *Electrochim. Acta* **2012**, *70*, 344.
(26) Mogi, R.; Inaba, M.; Jeong, S.-K.; Iriyama, Y.; Abe, T.; Ogumi, Z. Effects of some organic additives on lithium deposition in propylene carbonate. *J. Electrochem. Soc.* **2002**, *149*, A1578.
(27) Zheng, J.; Engelhard, M. H.; Mei, D.; Jiao, S.; Polzin, B. J.; Zhang, J.-G.; Xu, W. Electrolyte additive enabled fast charging and stable cycling lithium metal batteries. *Nat. Energy* **2017**, *2*, 17012.
(28) Cheng, X.-B.; Zhao, M.-Q.; Chen, C.; Pentecost, A.; Maleski, K.; Mathis, T.; Zhang, X.-Q.; Zhang, Q.; Jiang, J.; Gogotsi, Y. Nanodiamonds suppress the growth of lithium dendrites. *Nat. Commun.* **2017**, *8*, 336.
(29) Liu, Y.; Lin, D.; Liang, Z.; Zhao, J.; Yan, K.; Cui, Y. Lithium-coated polymeric matrix as a minimum volume-change and dendrite-free lithium metal anode. *Nat. Commun.* **2016**, *7*, 10992.
(30) Liu, Y.; Lin, D.; Yuen, P. Y.; Liu, K.; Xie, J.; Dauskardt, R. H.; Cui, Y. An artificial solid electrolyte interphase with high Li-ion conductivity, mechanical strength, and flexibility for stable lithium metal anodes. *Adv. Mater.* **2017**, *29*, 1605531.
(31) Yan, K.; Lu, Z.; Lee, H.-W.; Xiong, F.; Hsu, P.-C.; Li, Y.; Zhao, J.; Chu, S.; Cui, Y. Selective deposition and stable encapsulation of lithium through heterogeneous seeded growth. *Nat. Energy* **2016**, *1*, 16010.
(32) Liu, W.; Lin, D.; Pei, A.; Cui, Y. Stabilizing lithium metal anodes by uniform Li-ion flux distribution in nanochannel confinement. *J. Am. Chem. Soc.* **2016**, *138*, 15443.
(33) Zheng, G.; Lee, S. W.; Liang, Z.; Lee, H.-W.; Yan, K.; Yao, H.; Wang, H.; Li, W.; Chu, S.; Cui, Y. Interconnected hollow carbon nanospheres for stable lithium metal anodes. *Nat. Nanotechnol.* **2014**, *9*, 618.
(34) Zeng, Z.; Liang, W.-I.; Liao, H.-G.; Xin, H. L.; Chu, Y.-H.; Zheng, H. Visualization of electrode−electrolyte interfaces in $LiPF_6$/EC/DEC electrolyte for lithium ion batteries via in situ TEM. *Nano Lett.* **2014**, *14*, 1745.
(35) Sacci, R. L.; Black, J. M.; Balke, N.; Dudney, N. J.; More, K. L.; Unocic, R. R. Nanoscale imaging of fundamental Li battery Chemistry: solid-electrolyte interphase formation and preferential growth of lithium metal nanoclusters. *Nano Lett.* **2015**, *15*, 2011.
(36) Bhattacharyya, R.; Key, B.; Chen, H.; Best, A. S.; Hollenkamp, A. F.; Grey, C. P. In situ NMR observation of the formation of metallic lithium microstructures in lithium batteries. *Nat. Mater.* **2010**, *9*, 504.
(37) Harry, K. J.; Hallinan, D. T.; Parkinson, D. Y.; MacDowell, A. A.; Balsara, N. P. Detection of subsurface structures underneath dendrites formed on cycled lithium metal electrodes. *Nat. Mater.* **2014**, *13*, 69.
(38) Wang, C.; Gong, Y.; Dai, J.; Zhang, L.; Xie, H.; Pastel, G.; Liu, B.; Wachsman, E.; Wang, H.; Hu, L. In Situ Neutron Depth Profiling of Lithium Metal−Garnet Interfaces for Solid State Batteries. *J. Am. Chem. Soc.* **2017**, *139*, 14257.
(39) Han, F.; Westover, A. S.; Yue, J.; Fan, X.; Wang, F.; Chi, M.; Leonard, D. N.; Dudney, N. J.; Wang, H.; Wang, C. High electronic conductivity as the origin of lithium dendrite formation within solid electrolytes. *Nat. Energy* **2019**, *4*, 187.
(40) Lv, S.; Verhallen, T.; Vasileiadis, A.; Ooms, F.; Xu, Y.; Li, Z.; Li, Z.; Wagemaker, M. Operando monitoring the lithium spatial distribution of lithium metal anodes. *Nat. Commun.* **2018**, *9*, 2152.
(41) Zhou, D.; Liu, R.; He, Y.-B.; Li, F.; Liu, M.; Li, B.; Yang, Q.-H.; Cai, Q.; Kang, F. SiO_2 Hollow Nanosphere-Based Composite Solid Electrolyte for Lithium Metal Batteries to Suppress Lithium Dendrite Growth and Enhance Cycle Life. *Adv. Energy Mater.* **2016**, *6*, 1502214.
(42) Ziegler, J. F.; Ziegler, M. D.; Biersack, J. P. SRIM − The stopping and range of ions in matter (2010). *Nucl. Instrum. Methods Phys. Res., Sect. B* **2010**, *268*, 1818.
(43) Oudenhoven, J. F. M.; Labohm, F.; Mulder, M.; Niessen, R. A. H.; Mulder, F. M.; Notten, P. H. L. In Situ Neutron Depth Profiling: A Powerful Method to Probe Lithium Transport in Micro-Batteries. *Adv. Mater.* **2011**, *23*, 4103.
(44) Liu, D. X.; Co, A. C. Revealing chemical processes involved in electrochemical (De)Lithiation of Al with in situ neutron depth profiling and X-ray diffraction. *J. Am. Chem. Soc.* **2016**, *138*, 231.
(45) Liu, D. X.; Wang, J.; Pan, K.; Qiu, J.; Canova, M.; Cao, L. R.; Co, A. C. In situ quantification and visualization of lithium transport with neutrons. *Angew. Chem.* **2014**, *53*, 9498.
(46) Zhang, X.; Verhallen, T. W.; Labohm, F.; Wagemaker, M. Direct Observation of Li-Ion Transport in Electrodes under Nonequilibrium Conditions Using Neutron Depth Profiling. *Adv. Energy Mater.* **2015**, *5*, 1500498.
(47) Liu, Z.; Verhallen, T. W.; Singh, D. P.; Wang, H.; Wagemaker, M.; Barnett, S. Relating the 3D electrode morphology to Li-ion battery performance; a case for $LiFePO_4$. *J. Power Sources* **2016**, *324*, 358.
(48) Nagpure, S. C.; Downing, R. G.; Bhushan, B.; Babu, S. S. Discovery of lithium in copper current collectors used in batteries. *Scr. Mater.* **2012**, *67*, 669.
(49) Aurbach, D.; Daroux, M. L.; Faguy, P. W.; Yeager, E. Identification of surface films formed on lithium in propylene carbonate solutions. *J. Electrochem. Soc.* **1987**, *134*, 1611.
(50) Aurbach, D.; Ein-Ely, Y.; Zaban, A. The surface chemistry of lithium electrodes in alkyl carbonate solutions. *J. Electrochem. Soc.* **1994**, *141*, L1.
(51) Peled, E.; Golodnitsky, D.; Ardel, G. Advanced model for solid electrolyte interphase electrodes in liquid and polymer electrolytes. *J. Electrochem. Soc.* **1997**, *144*, L208.
(52) Liang, Z.; Zheng, G.; Liu, C.; Liu, N.; Li, W.; Yan, K.; Yao, H.; Hsu, P.-C.; Chu, S.; Cui, Y. Polymer nanofiber-guided uniform lithium deposition for battery electrodes. *Nano Lett.* **2015**, *15*, 2910.
(53) Peng, H.-J.; Huang, J.-Q.; Liu, X.-Y.; Cheng, X.-B.; Xu, W.-T.; Zhao, C.-Z.; Wei, F.; Zhang, Q. Healing High-Loading Sulfur Electrodes with Unprecedented Long Cycling Life: Spatial Heterogeneity Control. *J. Am. Chem. Soc.* **2017**, *139*, 8458.
(54) Zhou, G.; Paek, E.; Hwang, G. S.; Manthiram, A. Long-life Li/polysulphide batteries with high sulphur loading enabled by lightweight three-dimensional nitrogen/sulphur-codoped graphene sponge. *Nat. Commun.* **2015**, *6*, 7760.
(55) Bodenes, L.; Dedryvère, R.; Martinez, H.; Fischer, F.; Tessier, C.; Pérès, J.-P. Lithium-ion batteries working at 85 C: Aging phenomena and electrode/electrolyte interfaces studied by XPS. *J. Electrochem. Soc.* **2012**, *159*, A1739.
(56) Verma, P.; Maire, P.; Novák, P. A review of the features and analyses of the solid electrolyte interphase in Li-ion batteries. *Electrochim. Acta* **2010**, *55*, 6332.
(57) He, Y.-B.; Li, B.; Liu, M.; Zhang, C.; Lv, W.; Yang, C.; Li, J.; Du, H.; Zhang, B.; Yang, Q.-H.; Kim, J.-K.; Kang, F. Gassing in $Li_4Ti_5O_{12}$-based batteries and its remedy. *Sci. Rep.* **2012**, *2*, 913.
(58) He, Y.-B.; Liu, M.; Huang, Z.-D.; Zhang, B.; Yu, Y.; Li, B.; Kang, F.; Kim, J.-K. Effect of solid electrolyte interface (SEI) film on cyclic performance of $Li_4Ti_5O_{12}$ anodes for Li ion batteries. *J. Power Sources* **2013**, *239*, 269.

DOI: 10.1021/acs.chemmater.9b01325
Chem. Mater. 2019, 31, 4564−4574

(59) Li, Z.; Ganapathy, S.; Xu, Y.; Zhu, Q.; Chen, W.; Kochetkov, I.; George, C.; Nazar, L. F.; Wagemaker, M. Fe_2O_3 Nanoparticle Seed Catalysts Enhance Cyclability on Deep (Dis)charge in Aprotic Li—O_2Batteries. *Adv. Energy Mater.* **2018**, *8*, 1703513.
(60) Yao, K. P. C.; Kwabi, D. G.; Quinlan, R. A.; Mansour, A. N.; Grimaud, A.; Lee, Y.-L.; Lu, Y.-C.; Shao-Horn, Y. Thermal stability of Li_2O_2 and Li_2O for Li-air batteries: in situ XRD and XPS studies. *J. Electrochem. Soc.* **2013**, *160*, A824.
(61) Park, K.; Goodenough, J. B. Dendrite-Suppressed Lithium Plating from a Liquid Electrolyte via Wetting of Li_3N. *Adv. Energy Mater.* **2017**, *7*, 1700732.
(62) Lin, D.; Zhao, J.; Sun, J.; Yao, H.; Liu, Y.; Yan, K.; Cui, Y. Three-dimensional stable lithium metal anode with nanoscale lithium islands embedded in ionically conductive solid matrix. *Proc. Natl. Acad. Sci. U. S. A.* **2017**, *114*, 4613.
(63) Zhang, S. S. A new finding on the role of $LiNO_3$ in lithium-sulfur battery. *J. Power Sources* **2016**, *322*, 99.
(64) Zhang, A.; Fang, X.; Shen, C.; Liu, Y.; Zhou, C. A carbon nanofiber network for stable lithium metal anodes with high Coulombic efficiency and long cycle life. *Nano Res.* **2016**, *9*, 3428.
(65) Zhuang, G. V.; Xu, K.; Yang, H.; Jow, T. R.; Ross, P. N. Lithium ethylene dicarbonate identified as the primary product of chemical and electrochemical reduction of EC in 1.2 M $LiPF_6$/EC: EMC electrolyte. *J. Phys. Chem. B* **2005**, *109*, 17567.

DOI: 10.1021/acs.chemmater.9b01325
Chem. Mater. 2019, 31, 4564−4574